Supporting Information for

Bioorthogonal Reaction-Mediated Photosensitizer-Peptide Conjugate Anchoring on Cell Membranes for Enhanced Photodynamic Therapy

Buwei Hu[1,3], Chenlin Ji[3,4], Zhuohang Zhou[3], Xuehan Xu[3,4], Luyi Wang[3,4], Tingting Cao[3,4], Jianjun Cheng[2,3,5*], Rui Sun[3,5*]

[1]Department of Materials Science, Fudan University, Shanghai 200433, China
[2]Research Center for Industries of the Future, Westlake University, Hangzhou, Zhejiang 310030, China
[3]School of Engineering, Westlake University, Hangzhou, Zhejiang 310023, China
[4]School of Material Science and Engineering, Zhejiang University, Hangzhou, Zhejiang 310023, China
[5]Institute of Advanced Technology, Westlake Institute for Advanced Study, Hangzhou, Zhejiang 310023, China

[*]Corresponding author.
E-mail: chengjianjun@westlake.edu.cn, sunrui14@westlake.edu.cn

Content

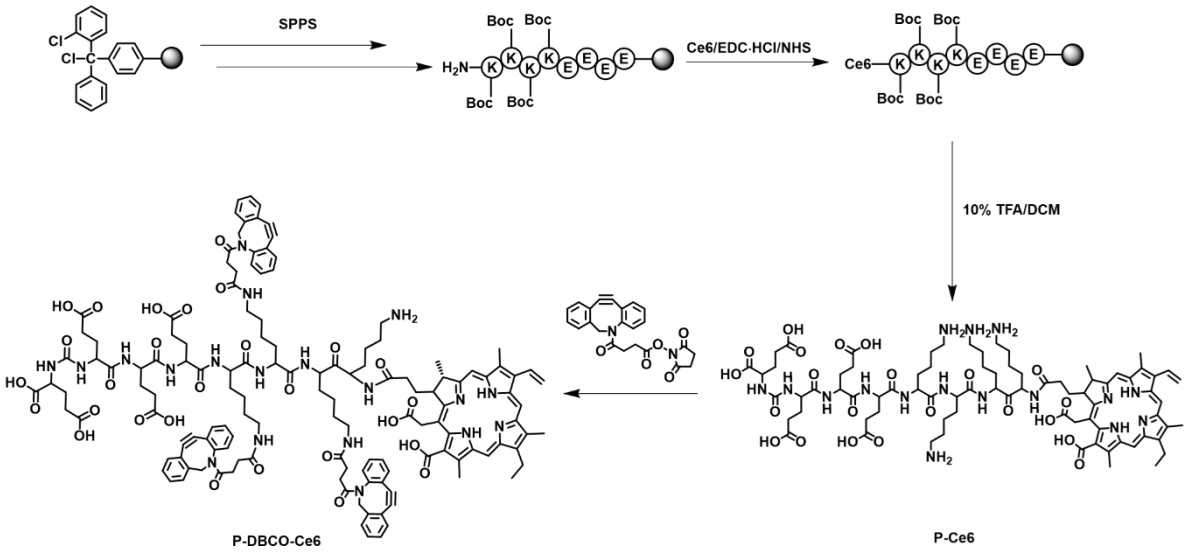

Figure S1. Synthesis scheme of P-Ce6 and P-DBCO-Ce6.

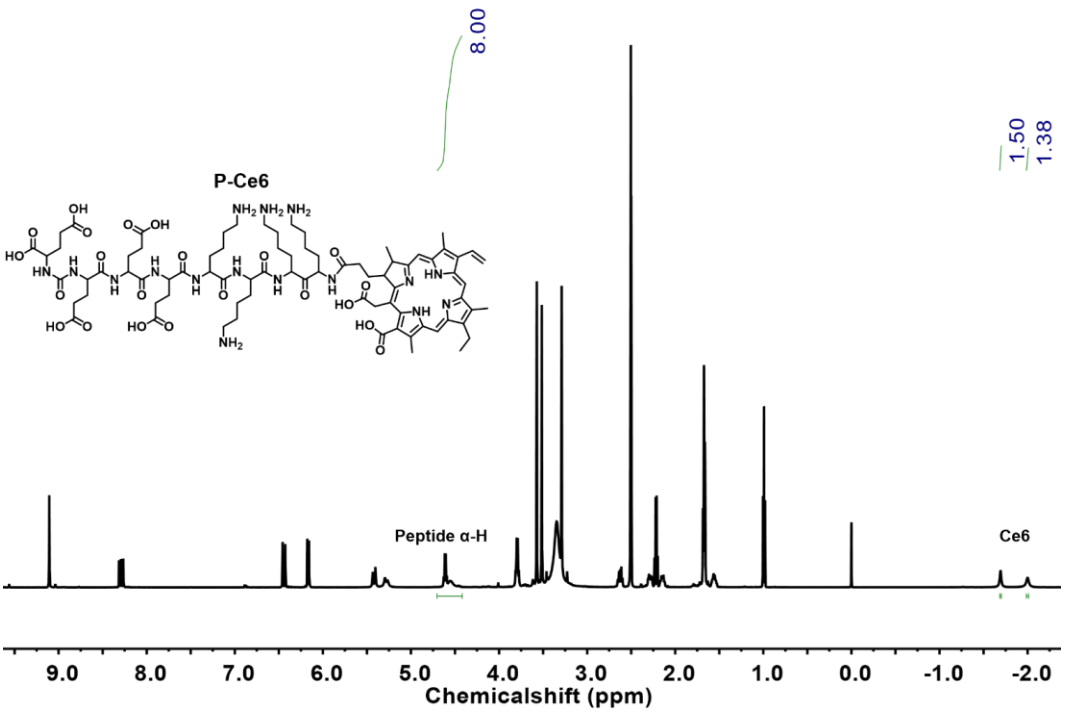

Figure S2. ^{1}H NMR Characterization of P-Ce6 in *d6*-DMSO.

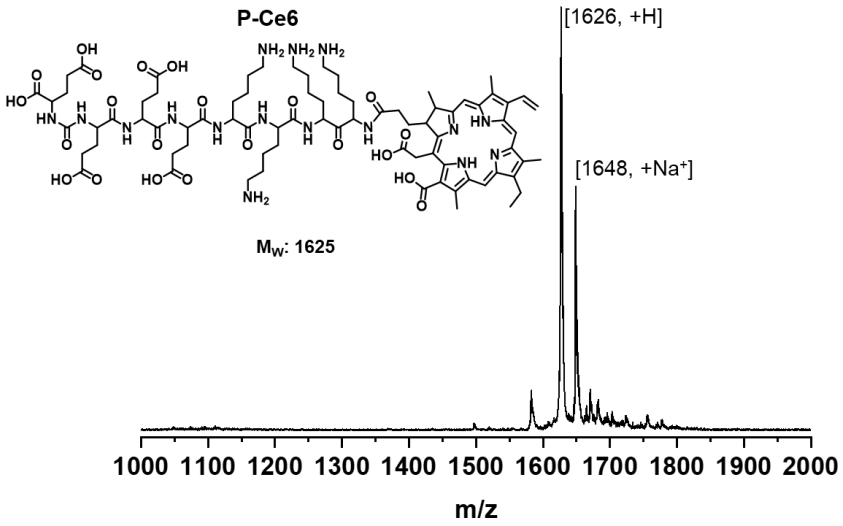

Figure S3. MALDI-TOF of P-Ce6 in CHCA matrix under LP model.

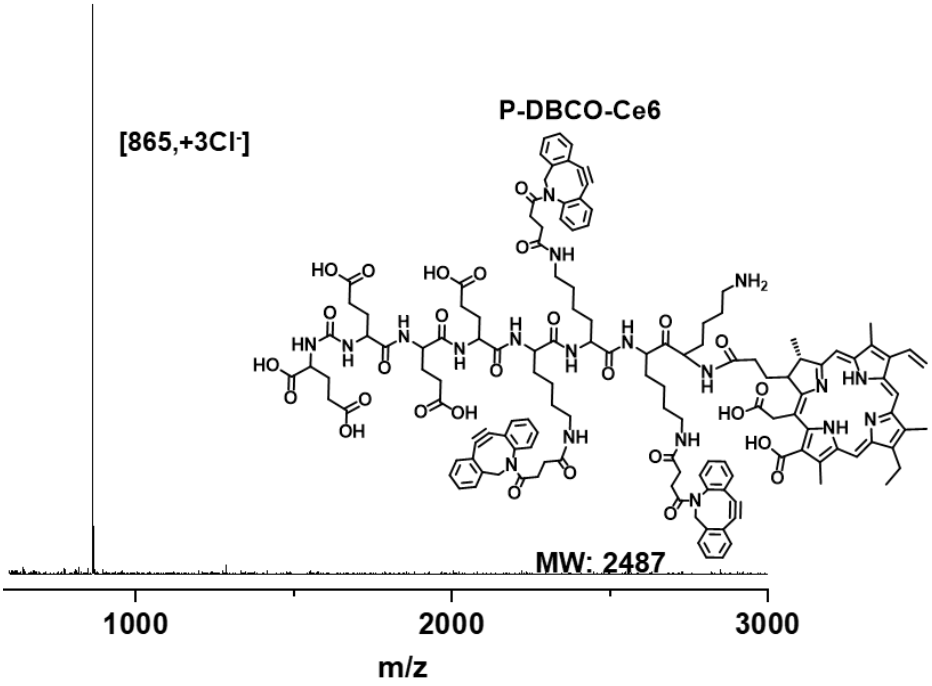

Figure S4. MALDI-TOF analysis of P-DBCO-Ce6 with DHB matrix under LN model.

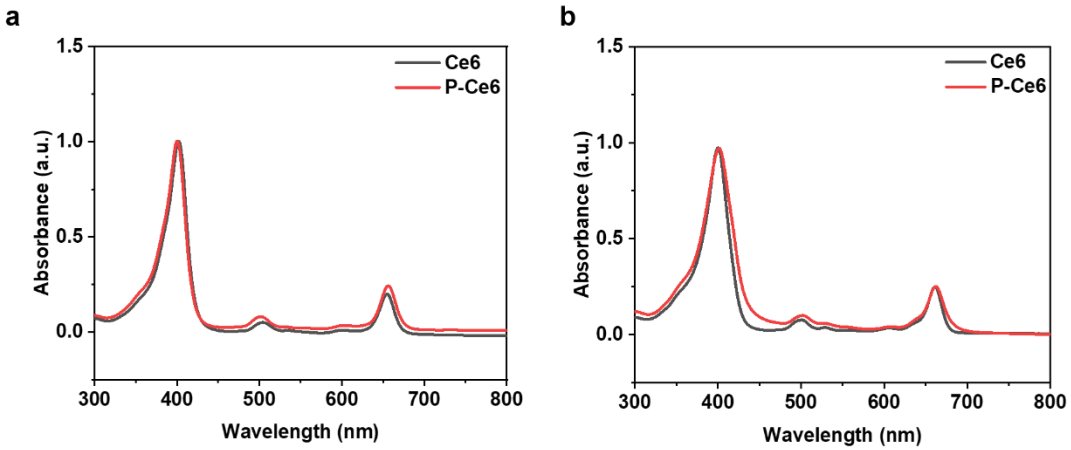

Figure S5. UV-Vis spectrum characterization of P-Ce6 in a) PBS and b) Methanol.

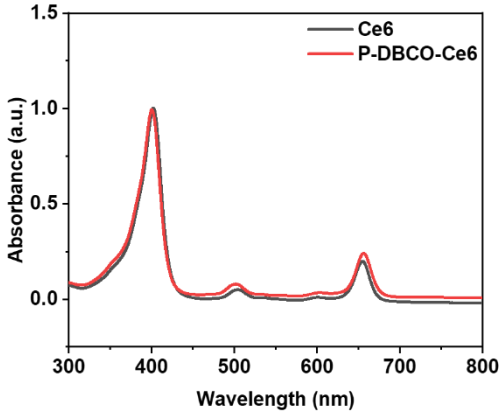

Figure S6. UV-Vis spectrum characterization of P-DBCO-Ce6 in PBS.

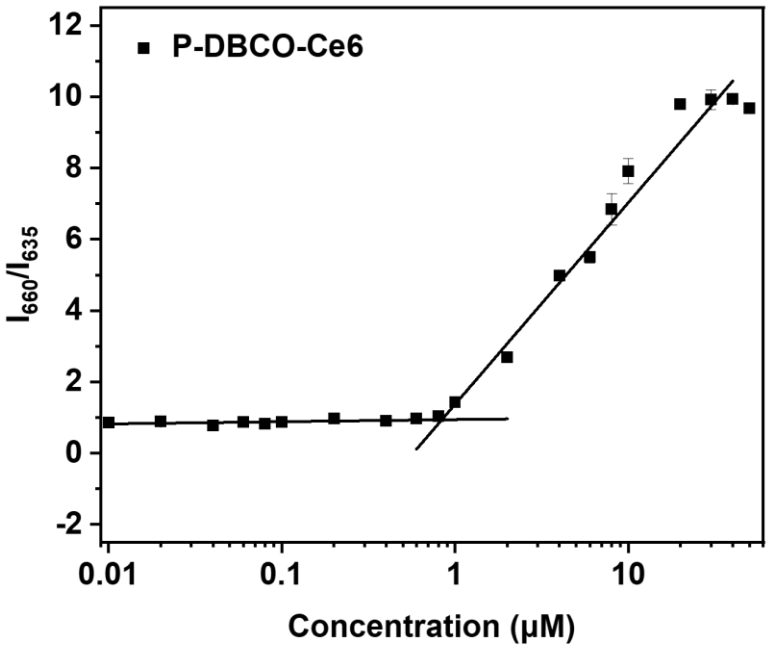

Figure S7. The critical micelle concentration (CMC) analysis of P-DBCO-Ce6 in PBS.

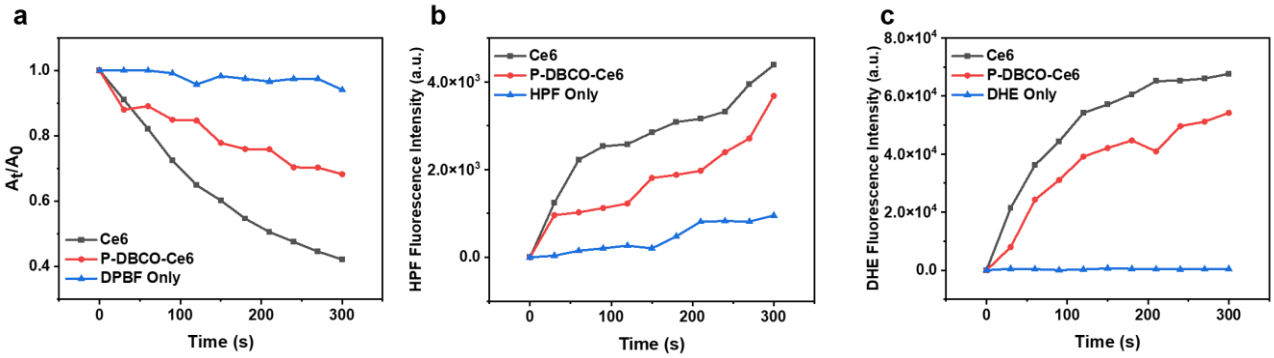

Figure S8. The generation of different types of reactive oxygen species (ROS) given by P-DBCO-Ce6 and Ce6, as detected by the corresponding probe. a) Degradation of DPBF, indicating the generation of singlet oxygen ($^1O_2$) by P-DBCO-Ce6 and Ce6 under laser irradiation for various time intervals; b) Generation of hydroxyl radicals (·OH) detected by HPF under laser irradiation; c) Time-dependent generation of superoxide anions ($O_2^{\cdot-}$) upon laser irradiation, as detected with DHE.

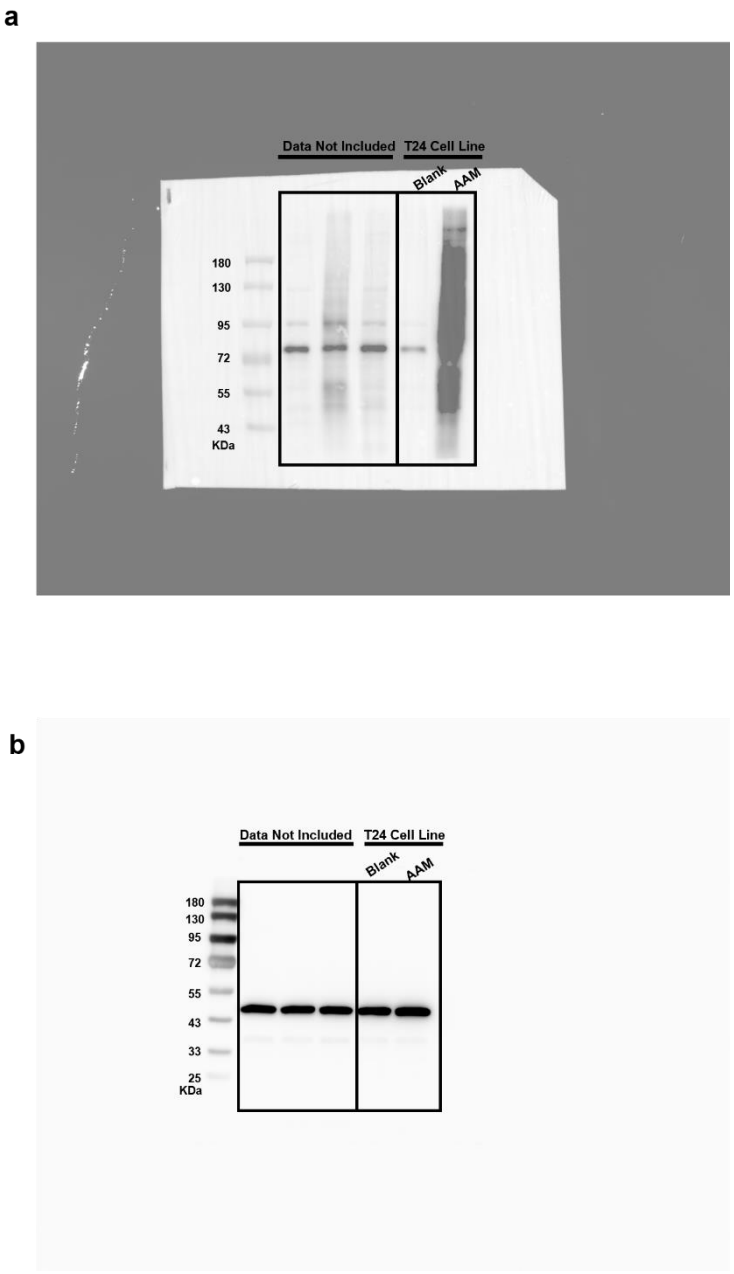

Figure S9. Western blot analysis of azide glycol labeling in T24 cells. a) Azide glycol labeling result; b) Actin of the corresponding sample.

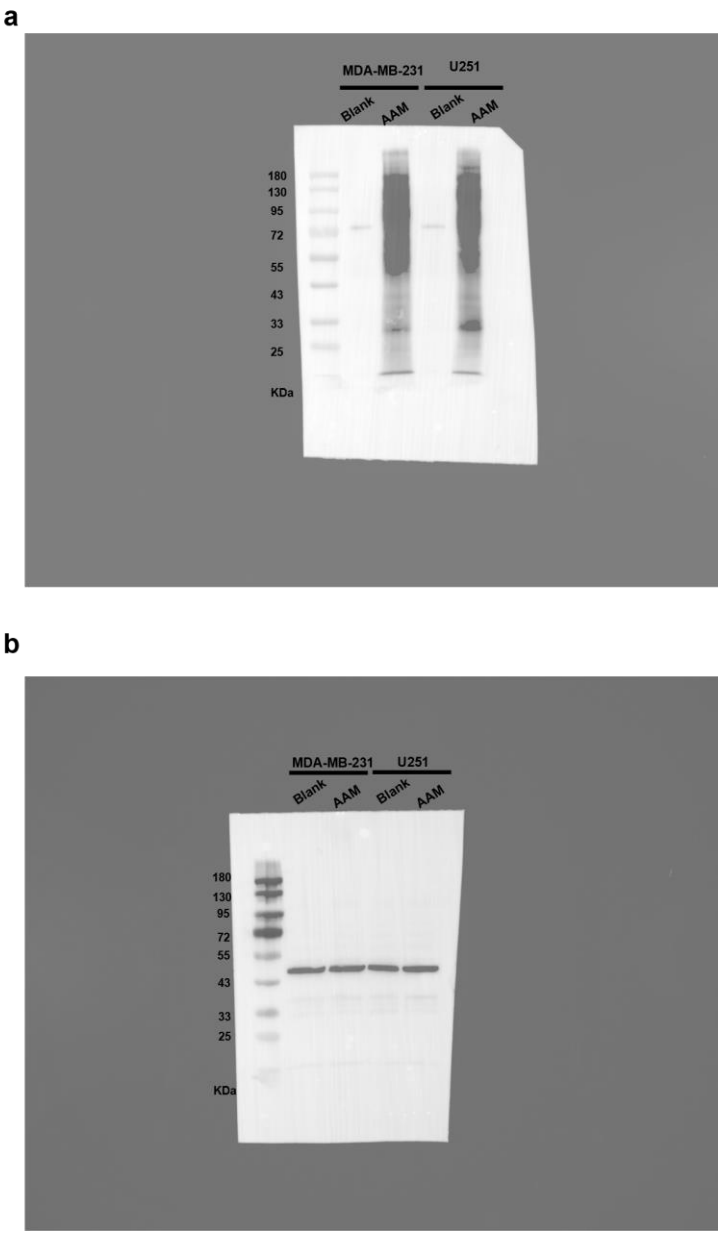

Figure S10. Western blot analysis of azide glycol labeling in U251 and MDA-MB-231 cells. a) Azide glycol labeling result; b) Actin of corresponding sample.

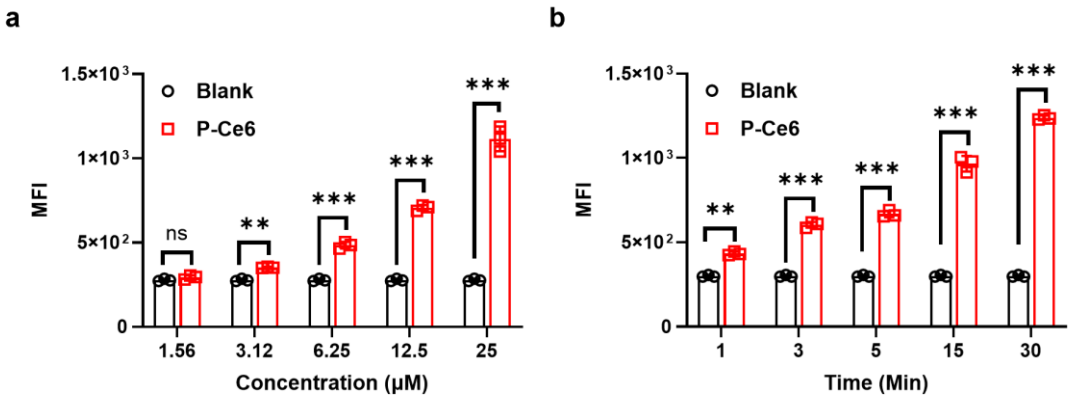

Figure S11. Cell surface absorption kinetics of P-Ce6 in T24 cells. a) The concentration-dependent cell attachment kinetic of P-Ce6, P-Ce6 incubated with cells for 30min; b) The time-dependent cell attachment kinetic of P-Ce6 (25 μM) (*p<0.05, **p<0.01, ***p<0.001).

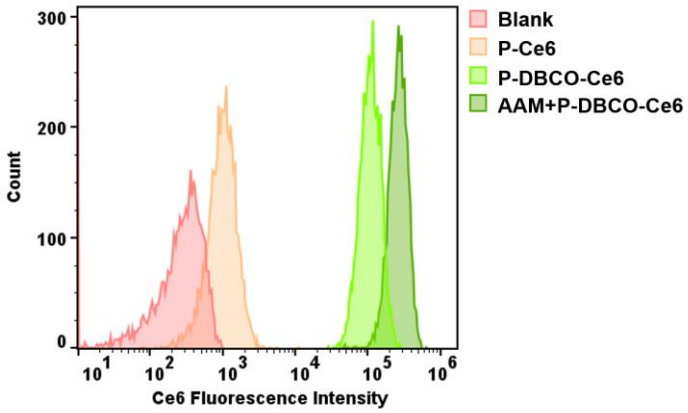

Figure S12. The cell surface attachment analysis of P-Ce6 and P-DBCO-Ce6. T24 cells were incubated with 25 μM of P-Ce6 or P-DBCO-Ce6 for 30 min under 37 ℃.

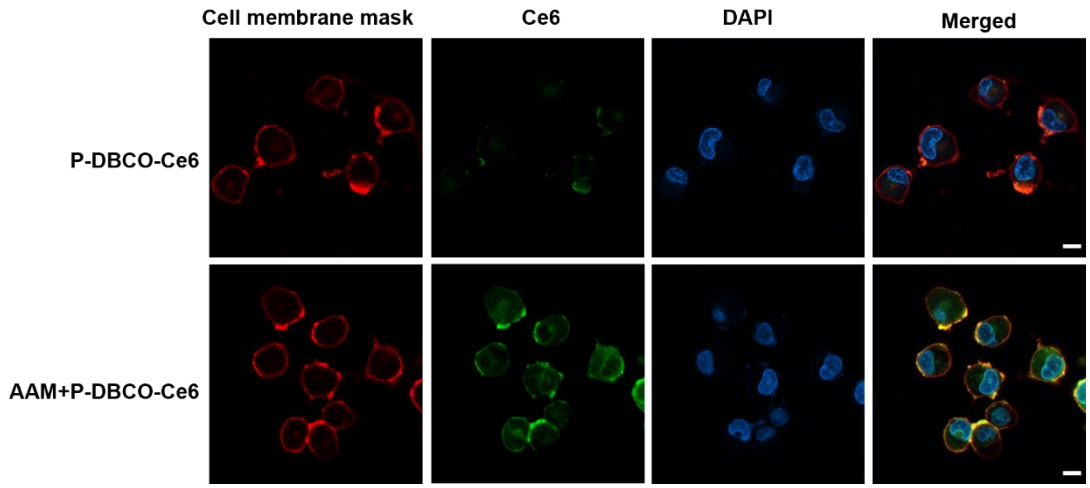

Figure S13. CLSM observation of P-DBCO-Ce6 cell membrane anchoring. T24 cells with or without AAM treatment were incubated with 50 μM of P-DBCO-Ce6 for 1 h under 37 ℃. Scale bar: 10μm.

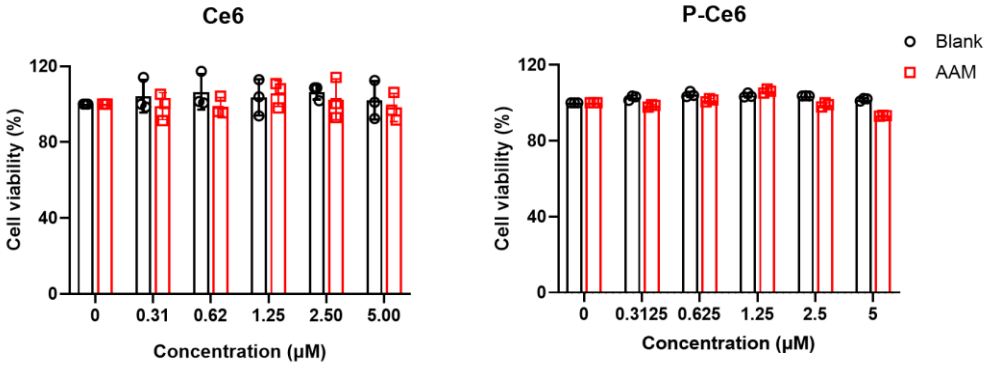

Figure S14. Phototoxicity assessment of Ce6 and P-Ce6 on T24 cells with or without AAM treatment. For phototoxicity, upon 660 nm laser irradiation, 10 mW/cm^2, 5 min.

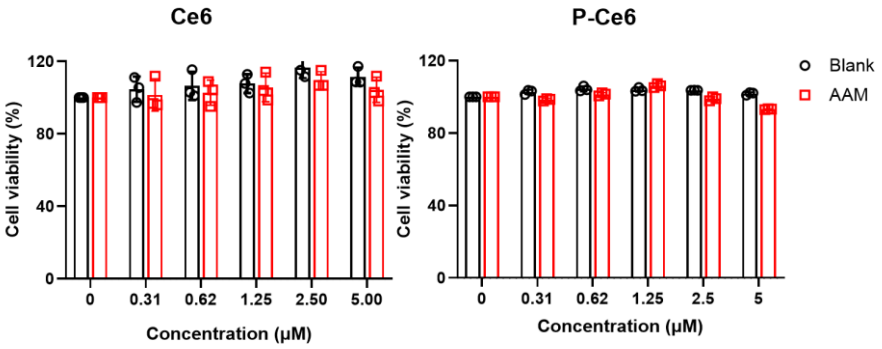

Figure S15. Dark toxicity assessment of Ce6 and P-Ce6 on T24 cells with or without AAM treatment.

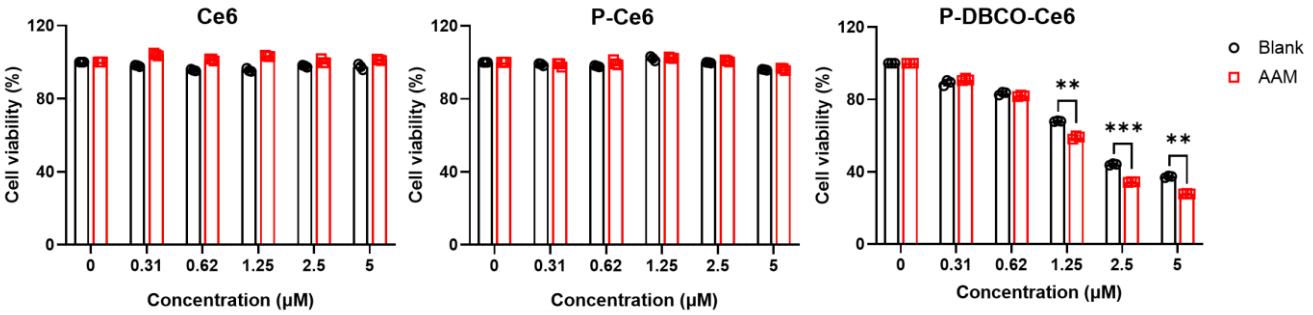

Figure S16. Phototoxicity assessment of Ce6, P-Ce6, and P-DBCO-Ce6 on MDA-MB-231 cells with or without AAM treatment. For phototoxicity, upon 660 nm laser irradiation, 10 mW/cm^2, 5 min (*p<0.05, **p<0.01, ***p<0.001).

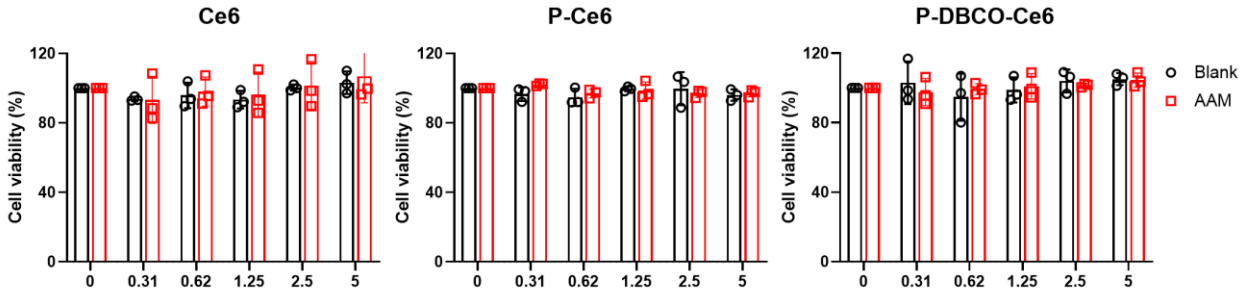

Figure S17. Dark toxicity assessment of Ce6, P-Ce6, and P-DBCO-Ce6 on MDA-MB-231 cells with or without AAM treatment.

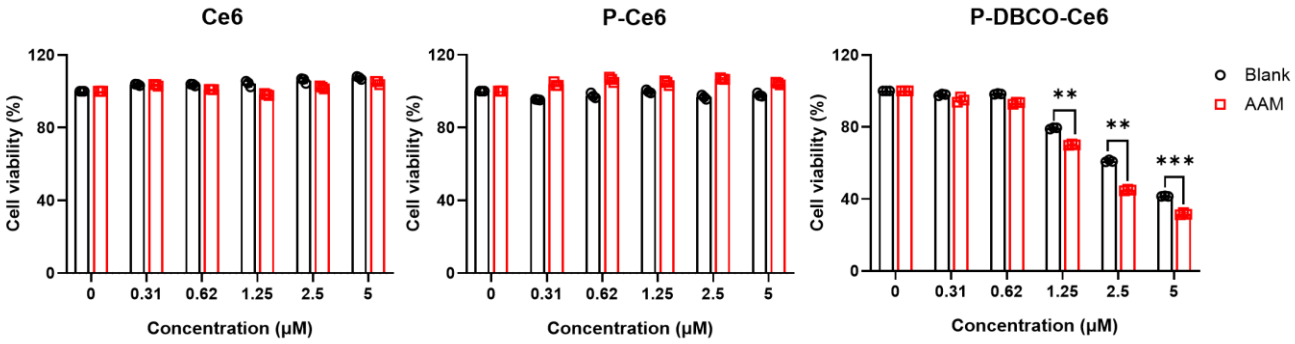

Figure S18. Phototoxicity assessment of Ce6, P-Ce6, and P-DBCO-Ce6 on U251 cells with or without AAM treatment. For phototoxicity, upon 660 nm laser irradiation, 10 mW/cm^2, 5 min (*p<0.05, **p<0.01, ***p<0.001).

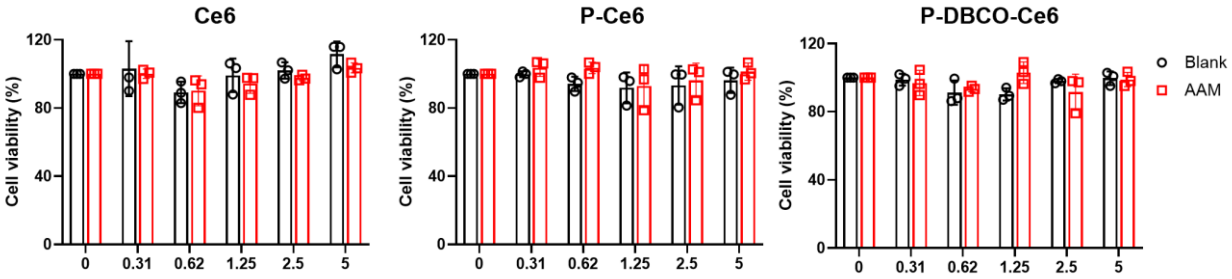

Figure S19. Dark toxicity assessment of Ce6, P-Ce6, and P-DBCO-Ce6 on U251 cells with or without AAM treatment.

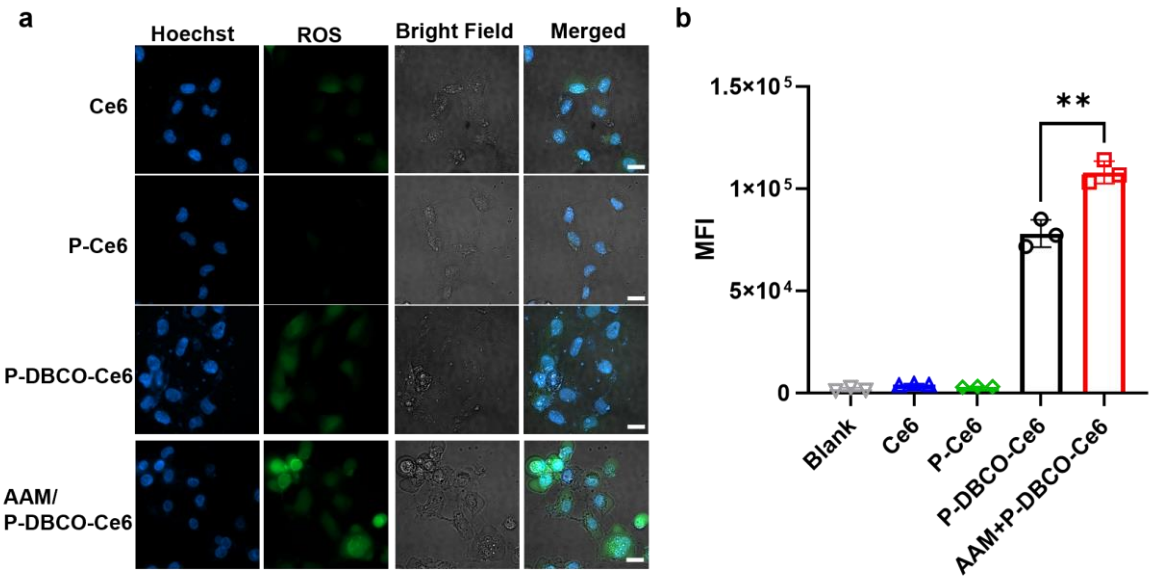

Figure S20. The intracellular ROS generation detected by a) ROS fluorescence probe imaged with CLSM and quantitatively analyzed with b) flow cytometry. T24 cells with or without AAM treatment were incubated with P-DBCO-Ce6, P-Ce6 or Ce6 (1 μM, 5 min), ROS detection was conducted after laser irradiation (*p<0.05, **p<0.01).

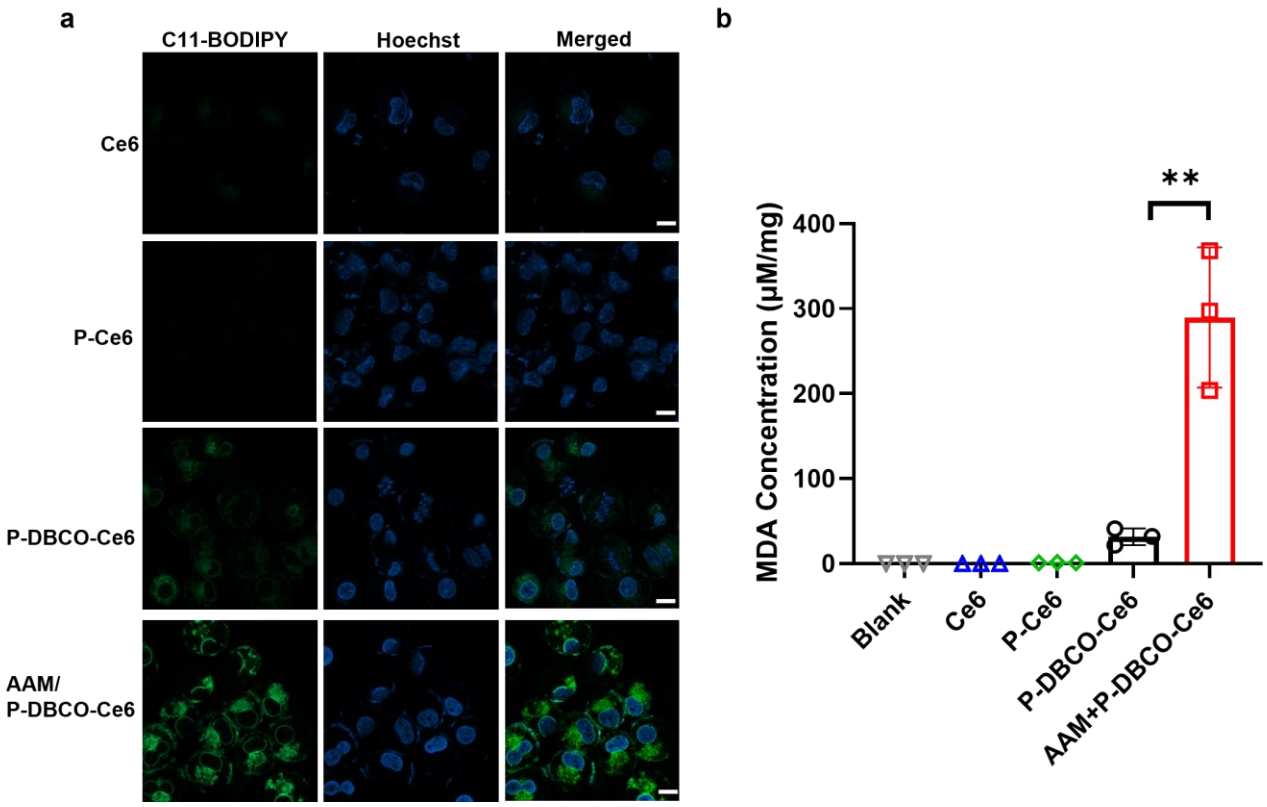

Figure S21. The cell membrane oxidation analysis. a) CLSM observation of C11-BODIPY excitation by ROS, generated from cell surface attached PS (25 μM, 10 min) under laser irradiation (40 mW/cm^2, 10 min); b) Intracellular MDA levels of cells with different treatment after laser irradiation (*p<0.05, **p<0.01).

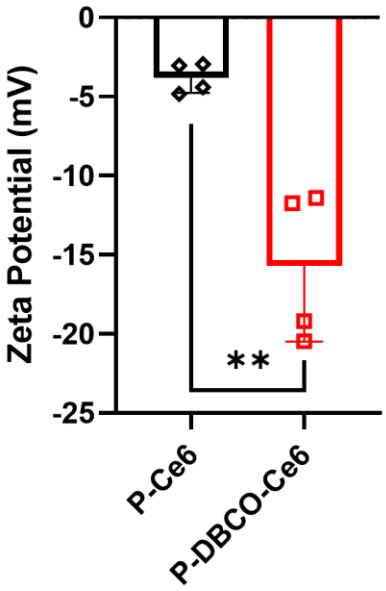

Figure S22. Zeta potential characterization of P-Ce6 & P-DBCO-Ce6 in PBS (*p<0.05, **p<0.01).

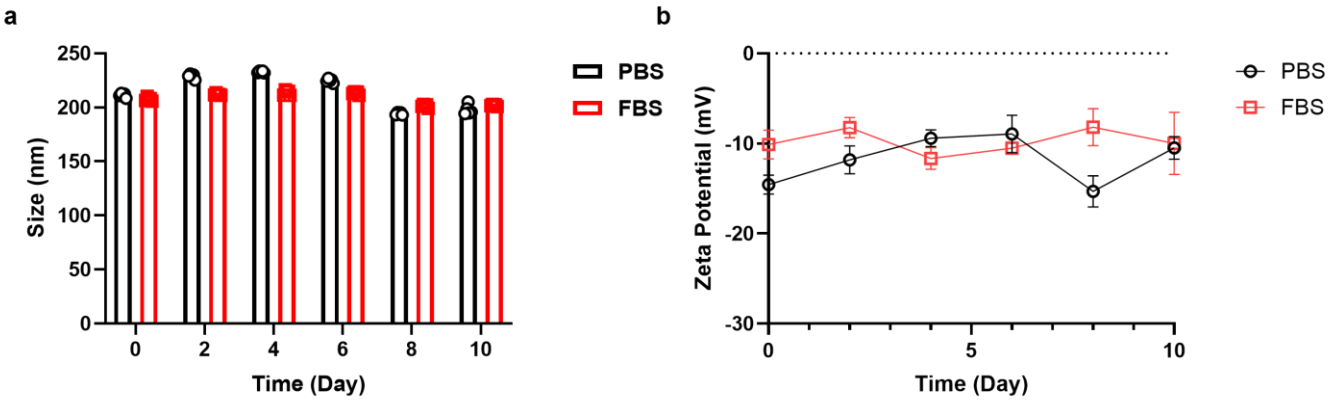

Figure S23. The AAM liposome stability assay: a) The size variation of AAM liposomes stored in PBS or 10% FBS at 4°C over different time intervals; b) ζ-potential changes of AAM liposomes under the same storage conditions.

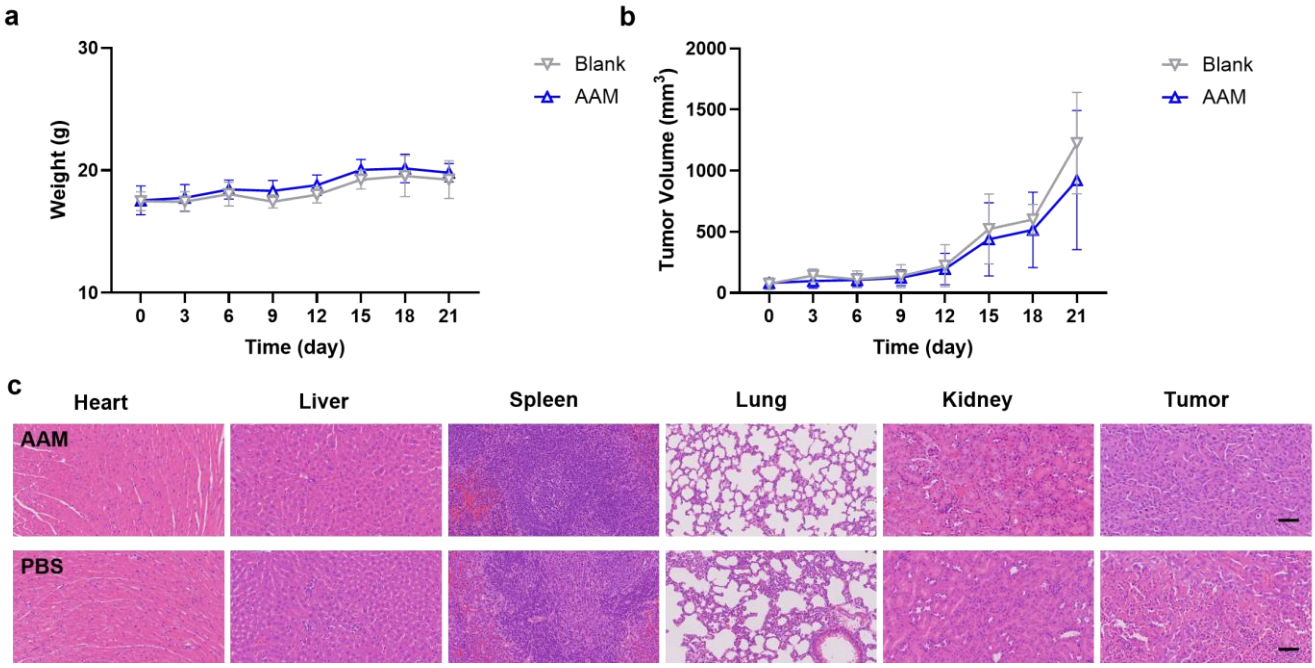

Figure S24. The AAM biosafety and tumor growth assay: a) The body weight of mice after received AAM or PBS; b) The tumor growth curve after administrate AAM or PBS; c) H&E staining of the major organ (heart, liver, spleen, lung and kidney) on day 21 after mice administrate AAM or PBS. Scale bar: 100μm.

Figure S25. Illustration of tumors harvested on day 21 after AAM or PBS administration.

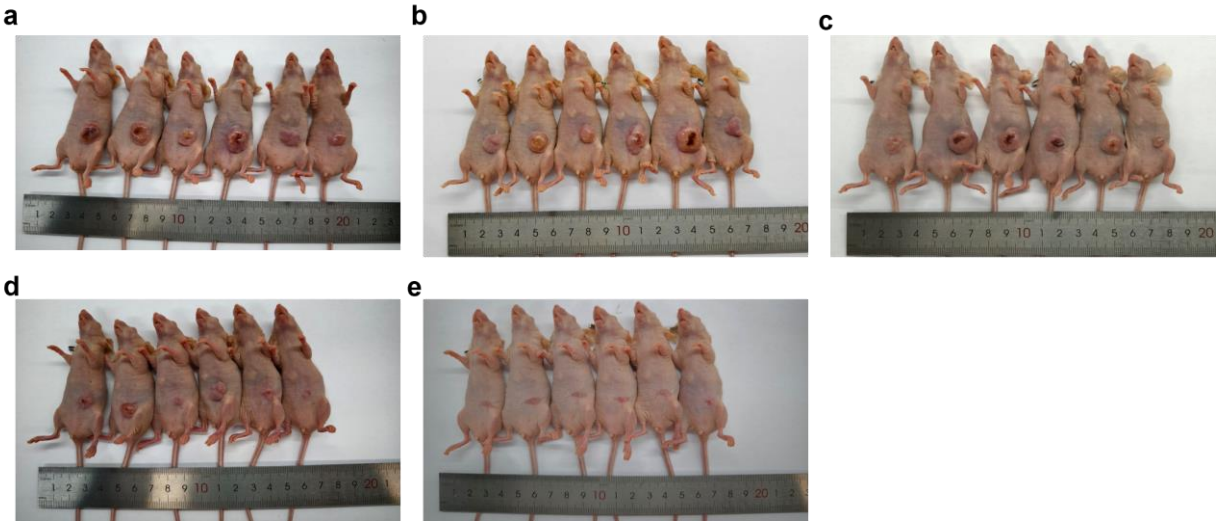

Figure S26. General illustration of T24-bearing mice on day 16 after PDT treatment. a) PBS; b) Ce6; c) P-Ce6; d) P-DBCO-Ce6; e) AAM + P-DBCO-Ce6.